Compact Engineering of Path-Entangled Sources from a Monolithic Quadratic Nonlinear Photonic Crystal

H. Jin,[1] P. Xu,[1,*] X. W. Luo,[1] H. Y. Leng,[1] Y. X. Gong,[2] W. J. Yu,[1] M. L. Zhong,[1] G. Zhao,[3] and S. N. Zhu[1]

[1]*National Laboratory of Solid State Microstructures, College of Physics, and National Center of Microstructures and Quantum Manipulation, Nanjing University, Nanjing 210093, China*

[2]*Department of Physics, Southeast University, Nanjing 211189, China*

[3]*College of Engineering and Applied Sciences, Nanjing University, Nanjing 210093, China*

(Received 28 February 2013; published 12 July 2013)

An integrated realization of photonic entangled states becomes an inevitable tendency toward integrated quantum optics. Here we report the compact engineering of steerable photonic path-entangled states from a monolithic quadratic nonlinear photonic crystal. The crystal acts as a coherent beam splitter to distribute photons into designed spatial modes, producing the heralded single-photon and appealing beamlike two-photon path entanglement. We characterize the path entanglement by implementing quantum spatial beating experiments. Such a multifunctional entangled source can be further extended to the high-dimensional fashion and multiphoton level, which paves a desirable way to engineering miniaturized quantum light sources.

DOI: 10.1103/PhysRevLett.111.023603 PACS numbers: 42.50.Dv, 42.50.St, 42.65.Lm, 77.84.Ek

Nowadays a consequent tendency toward practical quantum information processing is to manipulate photons including entangled photons on a monoplatform like an integrated waveguide chip [1–11]. However, most of the optical chips require external quantum light sources, which are usually bulky and involved with a lot of optical elements; thereby, as a further step toward integrated quantum optics, it is necessary to miniaturize the external light sources for improving their performance like multifunction, stability, and portability. A solid strategy for achieving integrated multifunctional quantum light sources turns to the traditional nonlinear optical crystals especially the domain-engineered quadratic nonlinear photonic crystals (NPC) [12,13]. By the domain-engineering technique, the spatial and temporal properties of entangled photons can be controlled inherently during the quasi-phase-matching (QPM) spontaneous parametric down-conversion (SPDC) processes [14–23], resulting in the generation of new types of photonic entanglement.

In this work, we mainly concentrate on the integrated engineering of single-photon and two-photon path-entangled states. The path entanglement is a valuable resource which applies the spatial mode to encode information, and has been harnessed for a variety of applications, such as quantum precise phase measurement [24,25] and super-resolution quantum lithography [26,27]. Even for the simple single-photon path entanglement [28–31], people also find interesting applications in quantum teleportation [32] and quantum networks [33]. However, for achieving path entanglement, extra endeavors should be paid after the entangled photons are generated from the nonlinear crystal. For example, a two-photon NOON state, i.e. a two-photon maximally path-entangled state $(|2,0\rangle + |0,2\rangle)/\sqrt{2}$, which can be usually generated by Hong-Ou-Mandel interference [1,34,35], requires a beam splitter to cascade after the crystal and hold on at a balanced position; therefore, integrated realization of such states is of essential importance.

Here we experimentally demonstrate the direct generation of single- and two-photon path-entangled sources from a monolithic domain-engineered NPC. Resulting from the concurrent multiple QPM SPDC processes, versatile spatial forms of down-converted beams are achieved and different types of photonic path-entangled states can be generated and transformed inside the same crystal wafer. Specifically, the heralded single-photon path entanglement can be steered into the beamlike two-photon path entanglement. We further demonstrate the valuable extension of such path-entangled states to the high-dimensional entanglement. These results present unique advantages of such monolithic domain-engineered crystals in the engineering of novel integrated quantum light sources, which are geared to integrated quantum optics.

Experimentally, a hexagonally poled lithium tantalate (HPLT) crystal is designed for the engineering of integrated path-entangled photon source. Figure 1(a) shows the micrograph of the etched congruent HPLT with the poling period $a = 7.507\ \mu$m, the crystal length $L =$ 18 mm and a reversal factor of $r/a \sim 28\%$ (r is the radius of round domain-inverted area), which is qualified for the efficient generation of degenerate 1064 nm photon pairs when the pump laser of 532 nm propagates along the y axis under a polarization configuration of $e \rightarrow e + e$. The quadratic nonlinear coefficient of our crystal can be expressed as Fourier series of $\chi^{(2)}(\vec{r}) = d_{33}\sum_{m,n} f_{m,n} e^{i\vec{G}_{m,n}\cdot\vec{r}}$ corresponding to a reciprocal lattice with sixfold symmetry as sketched in Fig. 1(b). Multiple reciprocal vectors $\vec{G}_{m,n}$ (m, n are integers) can ensure multiple QPM geometries for the entangled photons generation. In this work, we mainly

focus on $\vec{G}_{1,0}$ and $\vec{G}_{0,1}$, which have equal Fourier coefficients $f_{1,0} = f_{0,1} = 0.32$ [12]. The involved pair of QPM geometries follow $\vec{k}_p - \vec{G}_{1,0} - \vec{k}_s - \vec{k}_i = 0$ and $\vec{k}_p - \vec{G}_{0,1} - \vec{k}_s - \vec{k}_i = 0$, wherein $\vec{k}_p$, $\vec{k}_s$, and $\vec{k}_i$ are the wave vectors of the pump, signal, and idler photons, respectively. Generally, the photon pair will emit as either one of conical beams with principle axis along $\vec{k}_p - \vec{G}_{1,0}$ or $\vec{k}_p - \vec{G}_{0,1}$. Here only two types of concurrent processes are of our interest, which are depicted in Figs. 1(c) and 1(d), indicating the direct generation of single-photon and two-photon path-entangled states, respectively. In Fig. 1(c), two SPDC processes share the same idler mode which propagates collinearly with the pump, thereby, the corresponding signal photon belongs to either mode 1 (s_1) or mode 2 (s_2). Figure 1(d) shows the other case. Notably, in this case the photon pair emit together into beamlike modes which are desirable for the high-efficiency collection and high degree of path entanglement since $|1, 1\rangle$ term in this sample is prohibited by the QPM rule.

Under the first-order perturbation approximation [36], the two-photon state from concurrent two SPDC processes can be written as

$$|\psi\rangle = \Psi_0 \int d\omega_s \int d\omega_i \phi(\omega_s, \omega_i)[\hat{a}^\dagger_{s_1}(\vec{k}_{s_1})\hat{a}^\dagger_{i_1}(\vec{k}_{i_1}) + \hat{a}^\dagger_{s_2}(\vec{k}_{s_2})\hat{a}^\dagger_{i_2}(\vec{k}_{i_2})]|0\rangle, \quad (1)$$

in which Ψ_0 is a normalization constant, and the subscripts represent two different QPM processes. The two-photon mode functions of two processes take the same form $\phi(\omega_s, \omega_i) = \mathrm{sinc}(\Delta k_y L/2)\delta(\omega_p - \omega_s - \omega_i)$, wherein L is the length of the crystal, Δk_y is the phase mismatching in the longitudinal direction. Here, for a focused pump with 60 μm beam size, the longitudinal phase-matching condition takes the dominant role in the two-photon mode function, so we omit the transverse phase-matching part.

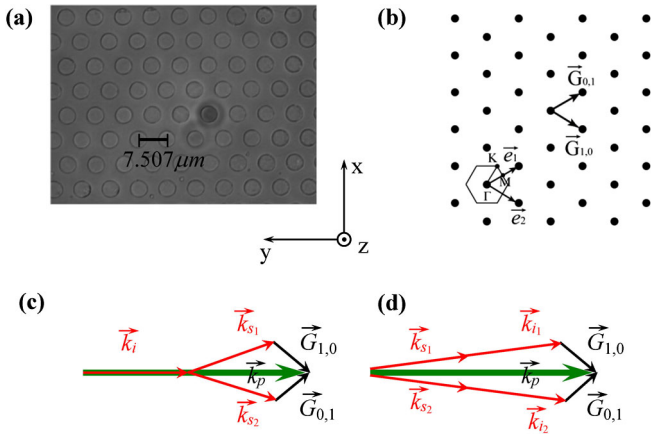

FIG. 1 (color online). (a) Micrograph of the etched congruent HPLT with dimensions of 18 mm × 6 mm × 0.5 mm. (b) The reciprocal lattice of the crystal. (c) and (d) are QPM conditions for the generation of single-photon and two-photon path entanglement, respectively.

For the single-photon path entanglement indicated in Fig. 1(c), we can take a partial trace of $\hat{\rho} = |\psi\rangle\langle\psi|$ [37], which is the density matrix operator of two-photon state, and write the density matrix of the signal as

$$\hat{\rho}_s = \Psi_0^2 \int d\upsilon |\phi(\upsilon)|^2 \Big[a^\dagger_{s_1}\Big(\frac{\omega_p}{2} + \upsilon\Big) + a^\dagger_{s_2}\Big(\frac{\omega_p}{2} + \upsilon\Big)\Big]|0\rangle\langle 0|\Big[a_{s_1}\Big(\frac{\omega_p}{2} + \upsilon\Big) + a_{s_2}\Big(\frac{\omega_p}{2} + \upsilon\Big)\Big], \quad (2)$$

in which we introduced a detuning frequency υ. The longitudinal phase mismatching in $\phi(\upsilon)$ can be written as

$$\Delta k_y = \frac{\upsilon(1 - \cos\theta_1)}{u_s} - \frac{\upsilon^2(1 + \cos\theta_1)}{2} \frac{d}{d\omega}\Big(\frac{1}{u}\Big)\Big|_{\omega=\omega_p/2},$$

wherein $u_s = \frac{d\omega}{dk}|_{\omega=\omega_p/2}$ is group velocity of signal and $\theta_1 = 2.192°$ is the angle between the wave vectors of signal and pump in the crystal. The bandwidth (FWHM) of signal photons is calculated to be 35.4 nm. Taking single-frequency approximation which can be guaranteed by narrowband interference filters, we can simplify Eq. (2) into

$$|\psi_1\rangle = \frac{1}{\sqrt{2}}(|1, 0\rangle + |0, 1\rangle), \quad (3)$$

which is a single-photon path-entangled state.

For the two-photon path entanglement indicated in Fig. 1(d), we can deduce the two-photon state to be

$$|\psi\rangle = \Psi_0 \int d\upsilon \phi(\upsilon)\Big[\hat{a}^\dagger_{s_1}\Big(\frac{\omega_p}{2} + \upsilon\Big)\hat{a}^\dagger_{i_1}\Big(\frac{\omega_p}{2} - \upsilon\Big) + \hat{a}^\dagger_{s_2}\Big(\frac{\omega_p}{2} + \upsilon\Big)\hat{a}^\dagger_{i_2}\Big(\frac{\omega_p}{2} - \upsilon\Big)\Big]|0\rangle. \quad (4)$$

In this case the phase mismatching is $\Delta k_y = -\upsilon^2 \cos\theta_2 \frac{d}{d\omega}(\frac{1}{u})|_{\omega=\omega_p/2}$, wherein $\theta_2 = 1.095°$ is the angle between the wave vectors of signal and pump. The theoretical bandwidth (FWHM) of down-converted photons is about 31.4 nm. Using single-frequency approximation, we can simplify Eq. (4) into

$$|\psi_2\rangle = \frac{1}{\sqrt{2}}(|2, 0\rangle + |0, 2\rangle), \quad (5)$$

which is a two-photon NOON state.

Figures 2(a)–2(d) record the spatial distribution evolution of down-converted photons generated from the HPLT when the temperature increased. Figures 2(b) and 2(d) disclose the spatial distribution of single-photon and two-photon path-entangled sources when the QPM conditions of Figs. 1(c) and 1(d) are satisfied, respectively. Although the coherence between two single- or two-photon modes is guaranteed physically by the coherence of concurrent nonlinear processes sharing the same pump, it is necessary to verify the path entanglement. Here we carry out spatial beating experiments to reveal quantum nature of the states by obtaining the fringe visibility and coherence length,

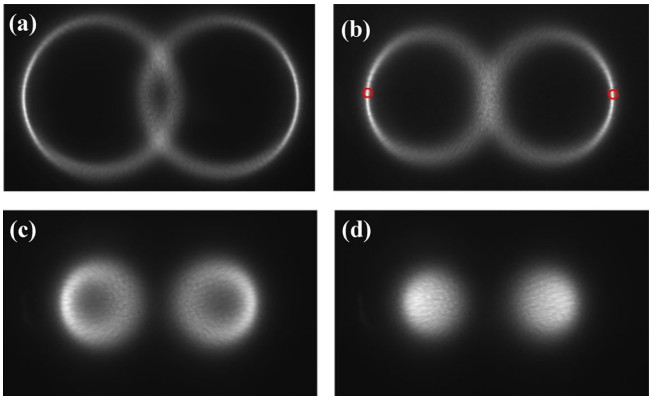

FIG. 2 (color online). (a) The spatial Fourier spectrum obtained at the focal plane of a convex lens when the crystal is set at 145 °C by a sensitive CCD camera. (b) The spatial Fourier spectrum at 154.6 °C. The two small red circles indicate the two modes of the single-photon entangled state. The angle between two signal modes outside of the crystal is measured to be about 9.54° which agrees well with the theoretical design of 9.38°. (c) The spatial Fourier spectrum at 168 °C. (d) The spatial Fourier spectrum at 172.3 °C. The two bright spots correspond to the noncollinear beamlike two-photon modes with the relative emitting angle outside of the crystal 4.88° (theoretically 4.69°). The measured divergence angle of each mode is about 2.26° (FWHM).

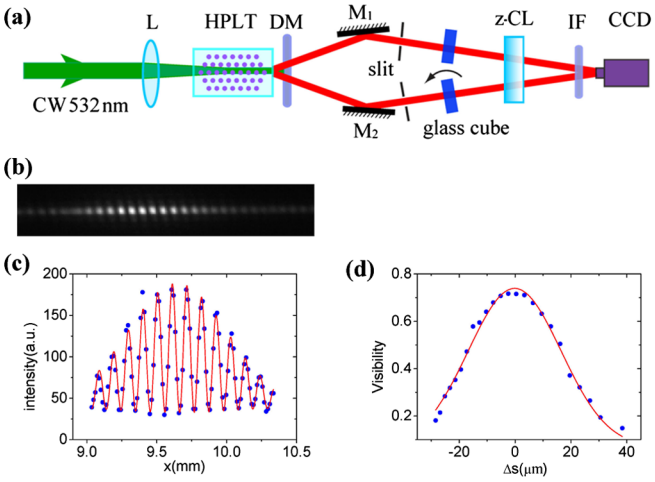

FIG. 3 (color online). (a) Experimental setup. The crystal is controlled at 154.6 °C and pumped with a cw single longitudinal mode 532 nm laser. After the crystal, the down-converted photons of 1064 nm are first separated from the pump by a dichromatic mirror DM, then two signal modes are both reflected by flat mirrors to ensure a small intersecting angle $2\theta = 10.4$ mrad so that the beating fringes can be resolved by the CCD camera which is sensitive to a few photons. A cylindrical lens z-CL gathers the intensity along the z axis. For each path, a 500 μm width slit (corresponding to an arc of 43 mrad on the ring of down-converted photons) is used to pick out the coherent signal mode. Preceding the CCD is a 40 nm bandwidth IF centered at 1064 nm. The optical path length of each mode is adjusted by rotating a K9 glass cube with 25.4 mm thickness. (b) The interference fringe observed by the CCD when the two modes have no optical path difference. (c) The intensity distribution extracted from Fig. 2(b). The solid red curve is sinusoidal fitting weighed by a Gaussian profile. (d) The relationship between the fringe visibility and the optical path-length difference.

which is equivalent to combining two single-photon or two-photon modes by a beam splitter but more stable since it is an integrated photonic setup.

At 154.6 °C, as shown in Fig. 2(b) the photon pair emit into either one of two tangent cones, resulting in the heralded single-photon path entanglement. Theoretically, when two coherent signal modes with wavelength λ intersect at an angle of 2θ, the spatial beating fringes will appear as

$$I_{\text{s.c.}} \propto 1 + \cos\left(\frac{2\pi x}{\lambda/(2\sin\theta)}\right). \tag{6}$$

Figure 3(a) shows the experimental setup. The coherent signal modes are picked out by two slits and intersect at an angle of $2\theta = 10.4$ mrad. Their beating fringes are recorded by a CCD camera which is sensitive to a few photons. In Figs. 3(b) and 3(c) we show the interference fringe when two optical paths are precisely controlled to be equal. The experimental data (blue dots) are fitted with a sinusoidal curve weighed by a Gaussian profile. The fitted curve shows a period of 104.4 μm, which agrees with the calculated value. The fringe visibility is 70.9%, which confirms that the two modes sketched in Fig. 1(c) are generated in a coherent way. The coherence is due to the indistinguishability of their idler modes. The coherence length, which is estimated by recording the relationship between the fringe visibility and the path difference as shown in Fig. 3(d), is measured to be 23.5 μm (the visibility drops to $1/e$), which fits well with theoretical value of 22.6 μm deduced from the theoretical single-photon bandwidth after taking the interference filter's (IF) transmission profile into account. When tuning the temperature away from 154.6 °C, two signal modes will share less of the idler mode and tend to be incoherent. At 143 °C, we find that the fringe visibility decreases to less than 30% under balanced path lengths of two modes.

As shown in Fig. 2(d), when the crystal is controlled at 172.3 °C, the photon pair will emit into either one of the bright well-defined beamlike spots, resulting in the two-photon path entanglement. Theoretically, the two-photon spatial correlation is proportional to

$$R_{\text{c.c.}} \propto 1 + \cos\left(\frac{2\pi x}{\lambda/(4\sin\theta)}\right) \tag{7}$$

when two two-photon modes intersect at an angle of 2θ. Two-photon beating fringes should present the period half of the single-photon case with the same wavelength. Figure 4(a) is the corresponding experimental setup for observing two-photon spatial beating fringe. As shown in Fig. 4(b) although the single counts of D_1 and D_2 show a smooth distribution, the coincidence counts reveal an interference fringe with the period of 48 μm, which consists

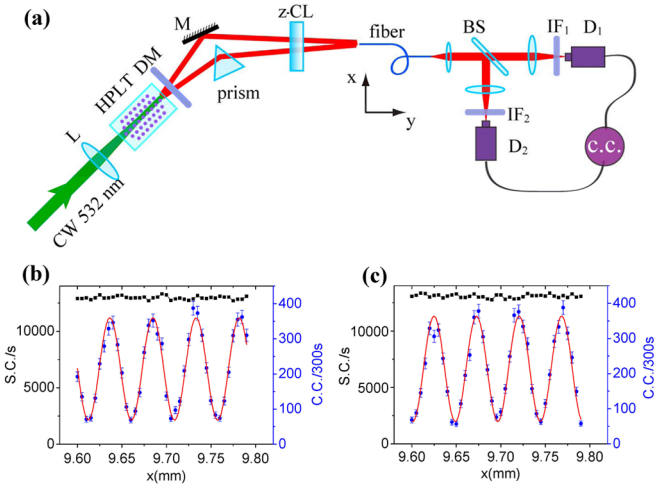

FIG. 4 (color online). (a) Experimental setup. The crystal temperature is controlled at 172.3 °C . A prism and a reflecting flat mirror are used to ensure that the two modes intersect at a small angle, and a cylindrical lens z-CL gathers the photons along the z axis into the fiber. The fiber tip is scanned along the x axis and cascaded by a coincidence counting measurement. Specifically, entangled photons are separated by a beam splitter (BS) after collimated by a lens and collected into two single photon detectors D_1 and D_2, respectively, by two lenses. The bandwidth of IF is 10 nm. (b) Measured single (black squares) and coincidence (blue dots) counts versus the transverse position of the fiber tip. The red solid line is sinusoidal fitting. (c) Measured single (black squares) and coincidence (blue dots) counts when one optical path length is extended by about 1 mm. Error bars show $\pm\sqrt{R_{\mathrm{c.c}}}$.

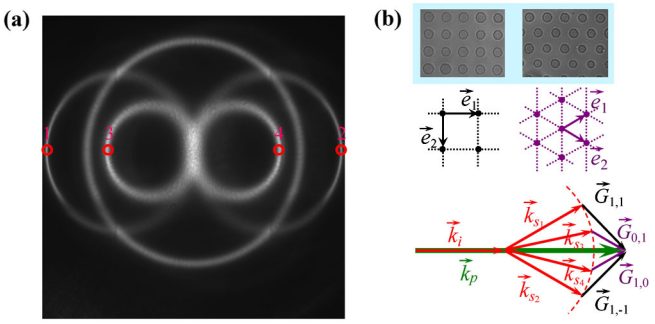

FIG. 5 (color online). (a) The spatial Fourier spectrum of 1064 nm photon pairs generated from a single domain-cascaded lithium niobate crystal. (b) Micrograph of the sample and involved four concurrent QPM conditions. Both domain blocks are ~6 mm long with a separation of 2 mm and each can supply a pair of reciprocal vectors ($\vec{G}_{1,1}$, $\vec{G}_{1,-1}$) for the tetragonal distribution with poling period of 6.271 μm or ($\vec{G}_{1,0}$, $\vec{G}_{0,1}$) for the hexagonal distribution with poling period of 6.445 μm.

well with Eq. (7) when $2\theta = 10.9$ mrad. The equivalent wavelength is reduced to $\lambda/2 = 532$ nm. The visibility of interference fringe is $68.2 \pm 1.8\%$, and it reaches $82.4 \pm 1.8\%$ when accidental coincidence counts are excluded from the raw data; therefore, the two-photon modes are coherently superposed. The nonideal visibility is caused by the nonperfect mode overlapping as well as the 1:2 intensity imbalance between the two modes since they go through different optical elements before the interaction. The intensity imbalance is valued through two-photon coincidence measurement for each mode by blocking the other one. Furthermore, to examine the two-photon coherence length which is theoretically determined by the pump, we increase the path difference by 1 mm which is much larger than the single photon coherence length of 113 μm (estimated by the 10 nm-bandwidth of IF) to find that the two-photon beating fringe [Fig. 4(c)] keeps almost the same visibility as in Fig. 4(b). For each beamlike mode, the conversion efficiency is $\sim 4.8 \times 10^{-10}$ when the pump power is 14 mW.

The spatial form of the down converted beams from the crystal is revealed to be controllable and versatile which exhibits the morphing behavior from two symmetric conical beams into two beamlike spots, resulting in the direct generation and easy switch of two types of path entanglement. It is worth noting that the spatial forms of photon pairs in Fig. 2 seem to be similar to those from some type-II birefringence-phase-matching (BPM) SPDC processes [38–40]; however, there exist intrinsic differences. The photon pair always emit into the same cone or beamlike spot in this work, while for BPM type-II cases the signal and idler photons usually emit into different ones. It is worth emphasizing that a recent work aiming to engineer the two-photon NOON state has just been published [18]. The results are similar to the two-photon case in this work; however, because of the parasitical SPDC process participated by the collinear reciprocal vector there exists an unwanted contribution of $|1, 1\rangle$ which causes some limitations.

Considering the state-of-the-art domain-engineered technique, such compact path-entangled states can be extended into the high-dimensional fashion and multiphoton level [17]. Figure 5 shows our experimental results in the realization of heralded single-photon high-dimensional path entanglement. Figure 5(a) is the spatial form of photon pairs generated from a single lithium niobate crystal wafer with cascaded tetragonally and hexagonally poled blocks. Each block can emit a heralded single-photon two-mode entangled state as Eq. (3). Since four concurrent SPDC processes share the same idler mode, the signal photon can emit into any one of modes 1, 2, 3, and 4 coherently as shown in Fig. 5(b). The single-photon multipartite entanglement can be written as

$$|\psi\rangle = \alpha(|1000\rangle + |0100\rangle) + \beta e^{i\varphi}(|0010\rangle + |0001\rangle). \quad (8)$$

α and β are decided by the SPDC efficiencies from each block. φ has a fixed value which relates with the length of each block and the interval between two blocks [41]. Following such a principle, the single-photon N-dimensional ($N \geq 5$) multipartite entanglement can further be approached. In addition, other degrees of freedom like polarization, orbital angular momentum, and frequency can also be manipulated inside the same crystal

chip, which will result in new types of compact photonic entanglement like hyperentanglement over several degrees of freedom. The integrated and miniaturized quantum light sources based on concurrent multiple QPM processes will act as a key element in exploring the knowledge boundaries of quantum mechanics and prompting the developments of practical quantum technologies.

The authors thank Z. Y. Ou for helpful discussions. This work was supported by the State Key Program for Basic Research in China (No. 2012CB921802 and No. 2011CBA00205), the National Natural Science Foundations of China (Contract No. 91121001, No. 11174121, No. 11021403, and No. 11004096), and the Project Funded by the Priority Academic Program development of Jiangsu Higher Education Institutions (PAPD), the Program for New Century Excellent Talents in University (NCET), and a Foundation for the Author of National Excellent Doctoral Dissertation of People's Republic of China (FANEDD).

*pingxu520@nju.edu.cn

[1] A. Politi, M. J. Cryan, J. G. Rarity, S. Yu, and J. L. O'Brien, Science **320**, 646 (2008).
[2] J. C. F. Matthews, A. Politi, A. Stefanov, and J. L. O'Brien, Nat. Photonics **3**, 346 (2009).
[3] B. J. Smith, D. Kundys, N. Thomas-Peter, P. G. R. Smith, and I. A. Walmsley, Opt. Express **17**, 13516 (2009).
[4] A. Politi, J. C. F. Matthews, and J. L. O'Brien, Science **325**, 1221 (2009).
[5] L. Sansoni, F. Sciarrino, G. Vallone, P. Mataloni, A. Crespi, R. Ramponi, and R. Osellame, Phys. Rev. Lett. **105**, 200503 (2010).
[6] A. Laing, A. Peruzzo, A. Politi, M. R. Verde, M. Halder, T. C. Ralph, M. G. Thompson, and J. L. O'Brien, Appl. Phys. Lett. **97**, 211109 (2010).
[7] M. F. Saleh, G. Di Giuseppe, B. E. A. Saleh, and M. C. Teich, Opt. Express **18**, 20475 (2010).
[8] A. Peruzzo, A. Laing, A. Politi, T. Rudolph, and J. L. O'Brien, Nat. Commun. **2**, 224 (2011).
[9] P. J. Shadbolt, M. R. Verde, A. Peruzzo, A. Politi, A. Laing, M. Lobino, J. C. F. Matthews, M. G. Thompson, and J. L. O'Brien, Nat. Photonics **6**, 45 (2011).
[10] J. C. F. Matthews, A. Politi, D. Bonneau, and J. L. O'Brien, Phys. Rev. Lett. **107**, 163602 (2011).
[11] D. Bonneau, M. Lobino, P. Jiang, C. M. Natarajan, M. G. Tanner, R. H. Hadfield, S. N. Dorenbos, V. Zwiller, M. G. Thompson, and J. L. O'Brien, Phys. Rev. Lett. **108**, 053601 (2012).
[12] V. Berger, Phys. Rev. Lett. **81**, 4136 (1998).
[13] N. G. R. Broderick, G. W. Ross, H. L. Offerhaus, D. J. Richardson, and D. C. Hanna, Phys. Rev. Lett. **84**, 4345 (2000).
[14] J. P. Torres, A. Alexandrescu, S. Carrasco, and L. Torner, Opt. Lett. **29**, 376 (2004).
[15] X. Q. Yu, P. Xu, Z. D. Xie, J. F. Wang, H. Y. Leng, J. S. Zhao, S. N. Zhu, and N. B. Ming, Phys. Rev. Lett. **101**, 233601 (2008).
[16] H. Y. Leng, X. Q. Yu, Y. X. Gong, P. Xu, Z. D. Xie, H. Jin, C. Zhang, and S. N. Zhu, Nat. Commun. **2**, 429 (2011).
[17] Y. X. Gong, P. Xu, Y. F. Bai, J. Yang, H. Y. Leng, Z. D. Xie, and S. N. Zhu, Phys. Rev. A **86**, 023835 (2012).
[18] E. Megidish, A. Halevy, H. S. Eisenberg, A. Ganany-Padowicz, N. Habshoosh, and A. Arie, Opt. Express **21**, 6689 (2013).
[19] S. Carrasco, J. P. Torres, L. Torner, A. Sergienko, B. E. A. Saleh, and M. C. Teich, Opt. Lett. **29**, 2429 (2004).
[20] S. E. Harris, Phys. Rev. Lett. **98**, 063602 (2007).
[21] M. B. Nasr, S. Carrasco, B. E. A. Saleh, A. V. Sergienko, M. C. Teich, J. P. Torres, L. Torner, D. S. Hum, and M. M. Fejer, Phys. Rev. Lett. **100**, 183601 (2008).
[22] S. Sensarn, G. Y. Yin, and S. E. Harris, Phys. Rev. Lett. **104**, 253602 (2010).
[23] A. M. Brańczyk, A. Fedrizzi, T. M. Stace, T. C. Ralph, and A. G. White, Opt. Express **19**, 55 (2010).
[24] T. Nagata, R. Okamoto, J. L. O'Brien, K. Sasaki, and S. Takeuchi, Science **316**, 726 (2007).
[25] J. W. Pan, Z. B. Chen, C. Y. Lu, H. Weinfurter, A. Zeilinger, and M. Żukowski, Rev. Mod. Phys. **84**, 777 (2012).
[26] A. N. Boto, P. Kok, D. S. Abrams, S. L. Braunstein, C. P. Williams, and J. P. Dowling, Phys. Rev. Lett. **85**, 2733 (2000).
[27] Y. Kawabe, H. Fujiwara, R. Okamoto, K. Sasaki, and S. Takeuchi, Opt. Express **15**, 14 244 (2007).
[28] S. M. Tan, D. F. Walls, and M. J. Collett, Phys. Rev. Lett. **66**, 252 (1991).
[29] L. Hardy, Phys. Rev. Lett. **73**, 2279 (1994).
[30] S. J. van Enk, Phys. Rev. A **72**, 064306 (2005).
[31] S. B. Papp, K. S. Choi, H. Deng, P. Lougovski, S. J. Van Enk, and H. J. Kimble, Science **324**, 764 (2009).
[32] G. Björk, A. Laghaout, and U. L. Andersen, Phys. Rev. A **85**, 022316 (2012).
[33] I. Usmani, C. Clausen, F. Bussières, N. Sangouard, M. Afzelius, and N. Gisin, Nat. Photonics **6**, 234 (2012).
[34] C. K. Hong, Z. Y. Ou, and L. Mandel, Phys. Rev. Lett. **59**, 2044 (1987).
[35] Y. H. Shih and C. O. Alley, Phys. Rev. Lett. **61**, 2921 (1988).
[36] M. H. Rubin, Phys. Rev. A **54**, 5349 (1996).
[37] D. V. Strekalov, Y. H. Kim, and Y. H. Shih, Phys. Rev. A **60**, 2685 (1999).
[38] P. G. Kwiat, K. Mattle, H. Weinfurter, A. Zeilinger, A. V. Sergienko, and Y. H. Shih, Phys. Rev. Lett. **75**, 4337 (1995).
[39] S. Takeuchi, Opt. Lett. **26**, 843 (2001).
[40] C. Kurtsiefer, M. Oberparleiter and H. Weinfurter, J. Mod. Opt. **48**, 1997 (2001).
[41] W. Ueno, F. Kaneda, H. Suzuki, S. Nagano, A. Syouji, R. Shimizu, K. Suizu, and K. Edamatsu, Opt. Express **20**, 5508 (2012).